Ultrasound in Med. & Biol. Vol. 18, No. 3, pp. 267–281, 1992
Printed in the U.S.A.

0301-5629/92 $5.00 + .00
© 1992 Pergamon Press Ltd.

●*Original Contribution*

ACOUSTIC EMISSION AND SONOLUMINESCENCE DUE TO CAVITATION AT THE BEAM FOCUS OF AN ELECTROHYDRAULIC SHOCK WAVE LITHOTRIPTER

A. J. COLEMAN, M. J. CHOI, J. E. SAUNDERS and T. G. LEIGHTON†
Medical Physics Department, St. Thomas' Hospital, London SE1 7EH and †Department of Physics, Cavendish Laboratory, Cambridge CB3 OHE, England

(*Received* 23 *July* 1991; *in final form* 30 *October* 1991)

Abstract—The acoustic emission from cavitation in the field of an extracorporeal shock wave lithotripter has been studied using a lead zirconate titanate piezoceramic (PC4) hydrophone in the form of a 100-mm diameter focused bowl of 120-mm focal length. With this hydrophone directed at the beam focus of an electrohydraulic lithotripter radiating into water, it is possible to identify signals well above the noise level, at the 1-MHz resonance of the hydrophone, which originate at the beam focus. Light emission, attributed to sonoluminescence, is also shown to originate at the focal region of the lithotripter, and the signal obtained from a fast photomultiplier tube directed at the focus has similarities in structure and timing to the detected acoustic signals. The multiple shock emission resulting from a single discharge of an electrohydraulic source is shown to result in two separate bursts of cavitational activity separated by a period of 3–4 ms. The signal burst corresponding to the primary shock has a duration of about 600 μs with little noticeable structure. The signal burst associated with the secondary shock has a reproducible structure with two distinct peaks separated by about 200 μs depending on the shock amplitude. The timing and structure of each burst is shown to be in reasonable agreement with the theoretical predictions made by Church (1989) based on the Gilmore model of bubble dynamics. In particular, it is shown that it is possible to obtain precise measurements of the time delay between the separate peaks within the signal burst detected following the secondary shock and this may, as predicted, provide a method of determining the size of bubbles remaining after the primary shock.

Key Words: **Lithotripsy, Ultrasonics, Cavitation.**

INTRODUCTION

The mechanisms by which the acoustic shock waves generated in extracorporeal shock wave lithotripsy (ESWL) interact with tissue and stone are poorly understood. Several studies, however, have reported evidence of acoustic cavitation occurring in water near the focus of lithotripters (Coleman et al. 1987; Riedlinger 1990), and cavitation is generally assumed to play some part in fragmenting stones (Koch and Grunewald 1989) and inducing biological effects in ESWL (Delius et al. 1990; Gambihler et al. 1990; Brummer et al. 1989). The ability to detect and quantify cavitation at the focus of a lithotripter is likely, therefore, to contribute to an understanding of the effectiveness and safety of the treatment, properties which have proved difficult to assess from the measurement of shock wave parameters alone.

Address correspondence to: A. J. Coleman.

A search for cavitation induced in blood within the abdominal aorta of dogs exposed to a lithotripsy field has been reported by Williams et al. (1989). This study employed a resonant bubble detector (RBD) (Miller 1981) and attributed the failure to detect bubbles to the inhibition of cavitation resulting from the high tensile strength of blood under *in vivo* conditions. Such a detector, however, may not provide the most appropriate measure of cavitation in lithotripsy since its design is based on the assumption that biological effects are induced primarily by resonant bubbles. While there is considerable evidence that this is true of low power cavitation (Nyborg and Miller 1982), biologically relevant cavitation is unlikely to be confined to stable bubbles of resonant size during lithotripsy exposures where high amplitude pulses are employed.

There are, in addition, some practical problems which limit the use of an active bubble detector such as the RBD in lithotripsy. Design considerations indi-

cate that both sending and receiving transducers of the RBD be situated within a few centimeters of the bubble field and that the bubbles be within a moving fluid (Miller 1981). In addition, the typical delay between generation and detection of bubbles is more than 0.5 s, and bubbles smaller than about 10 μm may redissolve in this time and go undetected. Detection of remnant bubbles of one size some time after the driving field has ceased may, therefore, not be expected to provide an accurate record of transient bubble activity induced by the high amplitude pulse from a lithotripter.

The acoustic emission from cavitation generated at the focus of an electrohydraulic shock wave source is examined, here, using a passive, focused hydrophone. Some of the advantages of this approach are discussed by Coakley (1971) and Gavrilov et al. (1988), and an early use of a directional hydrophone for cavitation detection is described by Hill et al. (1969). The present hydrophone can detect acoustic emission from transient cavitation induced by high amplitude pulses used in lithotripsy. It can be directed anywhere in the acoustic field from a position well outside the relatively violent lithotripter field and, being focused, also allows some spatial resolution. Its use is not restricted to examination of bubbles in moving fluids, and the device could conceivably provide information on cavitation occurring at depth within biological tissue. In lithotripsy, where bioeffects have been reported in tissues close to the beam focus, such a detector offers considerable advantages over an RBD.

Verification that the acoustic signal detected by this hydrophone arises from cavitation is attempted by comparing the hydrophone signal with that from a photomultiplier (PM) tube directed at the beam focus. Any light emission detected by the PM tube is attributed to cavitation-induced sonoluminescence (Walton and Reynolds 1984) and is taken as independent evidence that cavitation is present. A second experimental verification of the association between the detected acoustic signal and cavitation involves comparison of the signals obtained in tap water with those in carbonated water in which the violence of cavitational activity is expected to be reduced (Young 1989b).

Some of the predictions made in a theoretical study of lithotripsy-induced bubble dynamics by Church (1989) are summarized since they allow interpretation of the experimental measurements. The theoretical model used by Church (1989) has also been implemented to extend these predictions to account for the bubble dynamics in response to double shocks timed at about 3-ms intervals as are typically generated by electrohydraulic lithotripters.

THEORY

Introduction

The fundamental assumptions of the Gilmore model of bubble dynamics are that the bubble remains spherical throughout its motion, the radius of the bubble (R) is much smaller than the wavelength of the applied field, and the motion of the liquid surrounding the bubble is isentropic. Diffusion of air in and out of the bubble has been taken into account since this critically influences the bubble radius.

The wavelength associated with a typical lithotripsy pulse (with a centre frequency of around 150 kHz) is, as required, several orders of magnitude larger than the largest bubbles considered in this study. However, the assumption that the bubble remains spherical can be considered to apply only in advance of any violent collapse which may result from exposure to high amplitude lithotripsy pulses. Following such a collapse, the bubble may fragment. Flynn and Church (1984) have estimated the average number of bubbles resulting from such a collapse to be between 4 and 50 so that the final bubble radii achieved in practice can be expected to be between about 1.6 and 3.7 times smaller than those calculated here.

High speed photographic evidence (Riedlinger 1990) suggests that a bubble cloud extending 50 mm in the axial direction around the focus is formed in water as a result of exposure to an electrohydraulic lithotripter similar to the Dornier HM3 and it should be noted that the response of a bubble cloud will be likely to differ from that of a single bubble modeled here. Such differences may result, for example, from interaction between bubbles and the wide variation in the initial bubble radii. Nevertheless, some gross features of the model may apply for a bubble cloud.

The theoretical model as described by Church (1989) has been implemented on a Cray X-MP/28 supercomputer using a C-compiler (Unix operating system). With step size optimization, the program takes around 2 h to run for the examples considered here. Results are obtained in the form of the bubble radius variation with time $R(t)$ and as the pressure variation with time at the surface of the bubble $P(t)$ with the boundary conditions specified by the measured output of the shock wave source and an initial bubble radius assumed typical of tap water.

Boundary conditions

An important difference between the acoustic output of an electrohydraulic lithotripter and that of both piezoelectric and electromagnetic lithotripters results from the generation of a plasma bubble between the electrode pair which constitutes the electro-

hydraulic acoustic source. Oscillations of this bubble following a single "firing" of the source result in the emission of multiple, rather than single, shocks. Hydrophone measurements show successive shocked pulses of diminishing amplitude and asymmetry emitted at intervals of the order of milliseconds (Hunter et al. 1986).

Only the first two shocks are considered here and are identified as the "primary" and "secondary" shocks. The delay between primary and secondary shocks is sensitive to the discharge strength but is typically about 3 ms for a primary peak pressure, $p+$, of 50 MPa. The $p+$ of the secondary shock is assumed, on the basis of broadband hydrophone measurements, to be 40% of that of the primary.

For convenience, both primary and secondary shocks (Fig. 1) are assumed to have the same waveform, $p(t)$, and a suitable expression for this waveform (Church 1989) is given by:

$$p(t) = 2(p+)e^{-\alpha t}\cos(2ft + \pi/3).$$

For the primary pulse, α is chosen to be 8.0 10^5 s^{-1} and f is 83.3 kHz, giving a pulse with an asymmetry ratio ($p+/p-$) of 5 and, for the secondary shock, α is set at 4.2 10^5 s^{-1} with the same value of f to correspond with the measured asymmetry ratio of 2. The effect of pulse rise time is not modeled here since, for values typical of electrohydraulic sources (<30 ns), the bubble response as noted by Church (1989) is insensitive to the rise time.

The response of pre-existing bubble nuclei to the primary shock is calculated with $p+ = 50$ MPa (corresponding to a 25-kV setting), and the initial bubble radius $R_o = 3$ μm, which is assumed to be typical for the cavitation nuclei in tap water (Keller 1972). The effect of this choice of R_o (and the spread of radii about R_o) on the bubble dynamics is considered below. Diffusion is modeled assuming water to contain 6 moles/m^3 of dissolved air. The response of any bubbles to the secondary shock is calculated with $p+ = 20$ MPa and with an initial bubble radius corresponding to the final bubble radius following the primary shock.

Primary shock

From the plot of bubble radius, $R(t)$, in Fig. 2 it is noted that the bubble collapses as soon as it encounters the compression half-cycle of the primary shock. The bubble then proceeds to grow rapidly as the tensile part of the shock arrives. The entire duration of the shock wave is about 10 μs and any bubble response beyond $t = 10$ μs, therefore, takes place in the absence of a driving field. The initial rapid growth is followed by a relatively long period (of about 200 μs) where the bubble wall is nearly stationary. The bubble then collapses violently and, if it survives intact, will continue to rebound and collapse, according to the model, with a 30-μs period. Most of the diffusion of gas into the bubble occurs during the long period following the shock when the bubble remains expanded and the 3-μm bubble, considered here, grows to a final radius of about 60 μm.

The plot of $P(t)$ in Fig. 2 illustrates the acoustic pressure at the bubble wall. This plot indicates an ini-

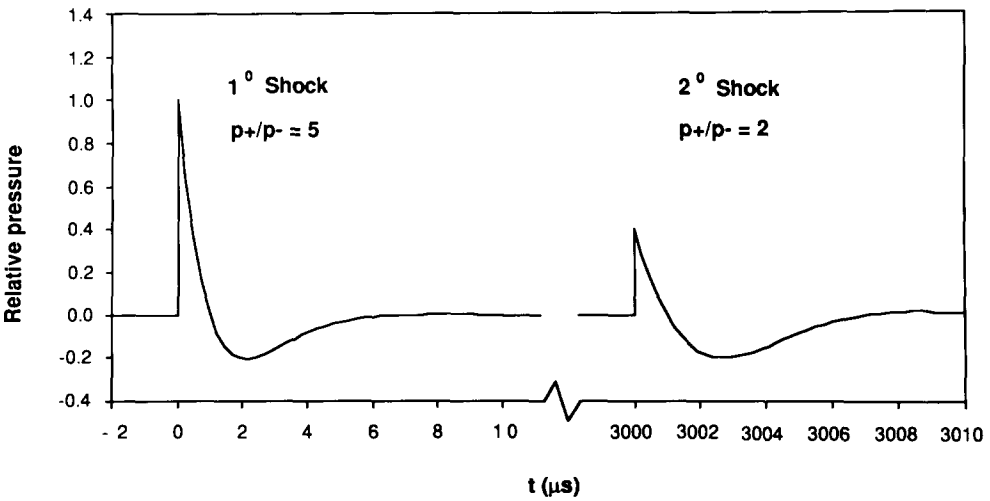

Fig. 1. The normalized pressure waveforms of the first two shocks emitted by an electrohydraulic lithotripter assumed in the theoretical model. Following a single discharge of the lithotripter, a primary shock (1°) of large amplitude (typically, $p+ = 50$ MPa) is followed some 3 ms later by a secondary shock (2°) of about 40% amplitude with a reduced asymmetry ratio. A third shock of considerably reduced amplitude is also occasionally observed but not considered here.

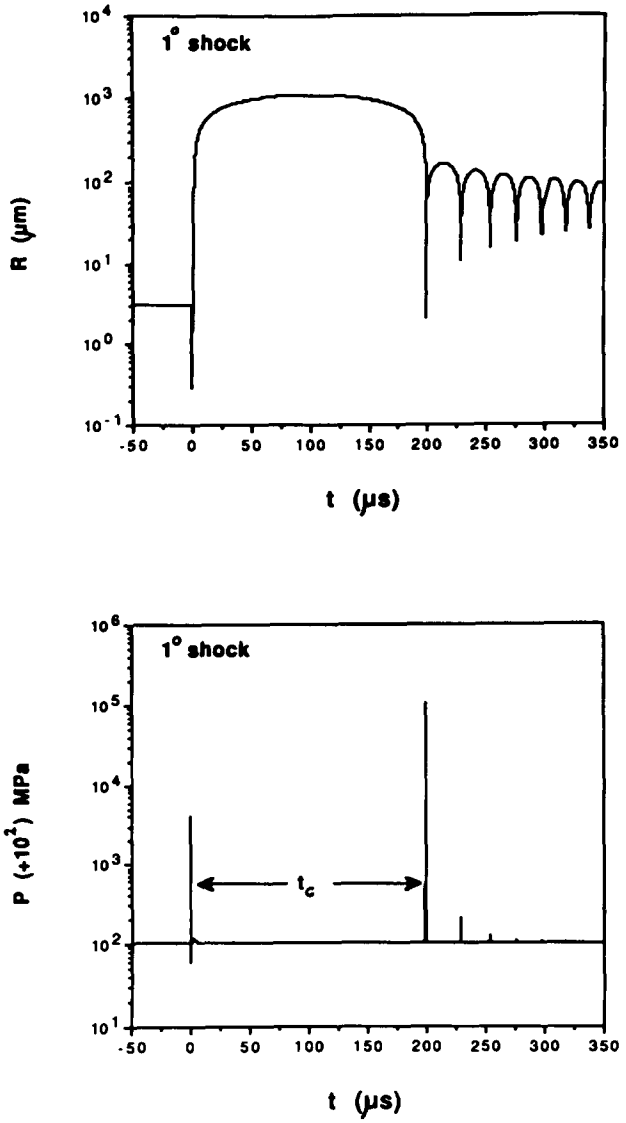

Fig. 2. The predicted bubble response to the primary (1°) shock. The bubble radius variation, $R(t)$, and pressure variation, $P(t)$, at the position of the bubble wall are plotted against time after the primary shock. The calculation assumes the waveform in Fig. 1 with $p+$ = 50 MPa and an initial bubble radius, R_o = 3 μm.

tial acoustic emission as the bubble collapses on encountering the shock wave at $t = 0$. There then follows a relatively long period, t_c, between the first and second bubble collapses where no acoustic output is expected and, finally, acoustic emission recommences as the second and subsequent collapses occur. The amplitude of the emission corresponding to the second collapse is a factor of about 10, higher than the initial emission at $t = 0$.

The dynamics of the bubble in response to the primary shock illustrated in Fig. 2 are essentially identical to those considered in detail by Church (1989). By varying the boundary conditions including, in particular, the shock amplitude ($p+$) and the initial bubble radius (R_o), Church has made some important observations concerning the predicted duration of the "quiet" period (t_c) and the radii of the bubbles immediately following the second collapse:

(a) The period t_c increases as a simple function of $p+$ and is weakly dependent on R_o.
(b) Measurement of t_c may provide a means of measuring R_o if $p+$ can be accurately determined.
(c) Any bubble with R_o between 1 and 10 μm will expand to the same (60 μm) final radius in response to a shock if $p+$ is sufficiently large.

Measurement of the time variation of the acoustic emission or sonoluminescence signal may be expected to provide a means of testing at least the first two predictions if signals above the noise level can be detected. The output of an electrohydraulic shock wave source offers an additional potential since the secondary shock, following within a few milliseconds of the primary shock, encounters the bubbles activated and enlarged by the primary shock.

Secondary shock

The bubble response to the secondary shock has been modeled, here, by assuming that this shock encounters a bubble with an initial radius (R_o = 60 μm) which has been enlarged (from 3 μm) as a result of diffusion following the primary shock. If bubble fragmentation takes place during the second (most violent) collapse initiated by the primary shock, as indicated by Flynn and Church (1984), the bubble population encountered by the secondary shock will still have a larger initial radius than that encountered by the primary shock but will be between about 16 μm and 38 μm rather than the value of 60 μm as used in the calculations generating the curves for $R(t)$ and $P(t)$ in Fig. 3.

The time variation of the bubble radius and wall pressure, $R(t)$ and $P(t)$, in response to the secondary shock (Fig. 3) have similar forms to those obtained for the primary shock (Fig. 2). The most notable difference is that diffusion is less significant in the secondary bubble response than in the response to the primary shock with the initial bubble radius (60 μm) remaining unchanged.

The plot of $P(t)$ for the secondary shock (Fig. 3) suggests that the pressure amplitude of the emission from the secondary shock may be expected to be smaller than from the primary shock, and the duration of the acoustically quiet period, t_c, following the secondary shock wave may be similar to that resulting from the primary shock.

Discussion

The maximum bubble wall velocity in the main collapse, $\dot{R}_{max}$, can be obtained from the data used to

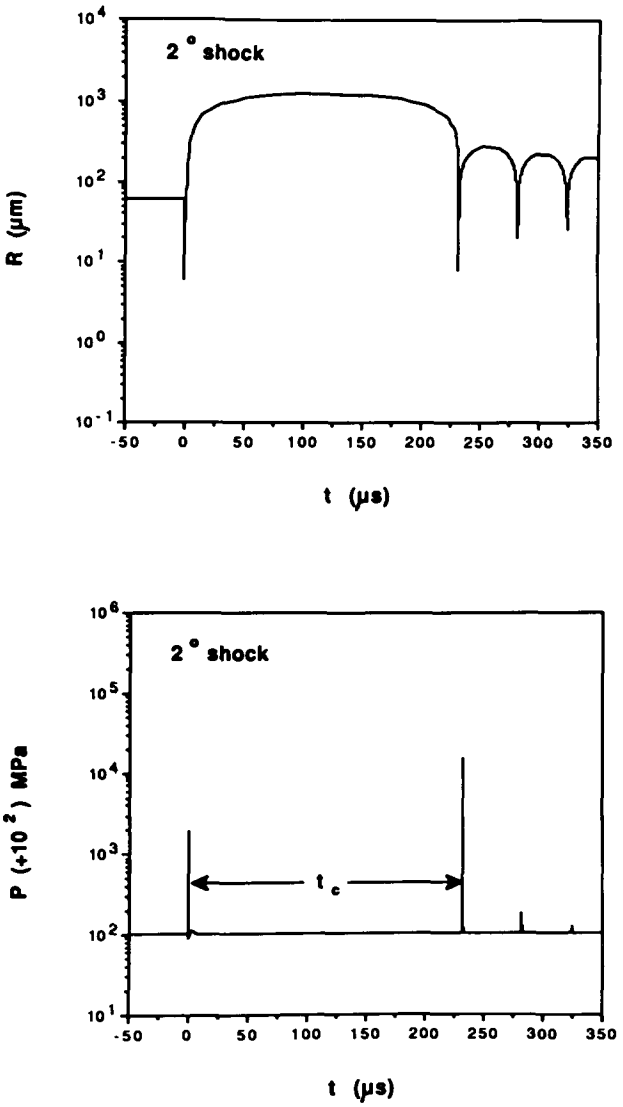

Fig. 3. The predicted bubble response to the secondary (2°) shock. The bubble radius, $R(t)$, and pressure variation, $P(t)$, at the bubble wall are plotted against time after the secondary shock. The calculation assumes, $p+ = 20$ MPa and an initial bubble size, $R_o = 60$ μm, this representing the bubble radius following the primary shock.

plot the graphs of $R(t)$ in Figs. 2 and 3, and $\dot{R}_{max}$ is greater than 2000 ms^{-1} and can achieve 4000 ms^{-1} if the bubble remains spherical. Since this exceeds the sound velocity in both water and air, shocks are therefore likely to be generated both in the gas within the bubble and the water surrounding it. The shocks in the water constitute the expected wideband acoustic emission from the bubble, and the formation of a shock in the gas within the bubble is taken as an indication that the processes within the bubble are possibly sufficiently violent for sonoluminescence production (Vaughan and Leeman 1986) so that the bubble may be expected to emit light. The amplitude of the pulse emitted at the second collapse of a single bubble (of initial radius 3 μm) in response to the primary shock is estimated to be about 1 MPa at a detector placed 120 mm from the bubble, as here.

The modeled behavior of a single bubble driven by a single lithotripter shock wave suggests that the emission of either sound or light will take the form of an initial burst immediately following the shock (at $t = 0$) followed by a "quiet" period of duration t_c. This period is predicted to last of the order of 200 μs, depending on the initial bubble radius and the amplitude of the driving shock pulse. Following this delay, there will be a second burst of emission corresponding to more violent bubble collapse. Subsequent behavior depends on whether or not the bubble fragments but will, in any case, consist of more rapid collapses and rebounds of steadily decreasing amplitude.

In practice, there will be a wide range of initial bubble sizes in tap water, and the acoustic emission from bubbles activated by the primary shock is likely to have a poorly defined quiet period as different size bubbles collapse out of phase. In addition, the high collapse pressure makes fragmentation of the bubbles more likely in response to the primary shock than in the secondary, increasing the variability in bubble dynamics which may result from primary shock exposure.

The prediction that any bubble with a radius between 1 and 10 μm will achieve the same final radius provided the shock amplitude is high (Church 1989) is particularly interesting. It suggests that bubble behaviour following the initial expansion period (t_c) progresses independently of the initial bubble radius. Most importantly, it implies that the secondary shock may encounter a narrower range of bubble sizes than the primary shock, and the detected acoustical and optical signal may be more coherent with a better resolved t_c.

METHOD

Shock wave sources

Two, nominally identical, electrohydraulic shock wave sources have been used in this study. Both have the same specifications which are based on those of the Dornier HM3 commercial lithotripter (having an 80 nF capacitance and a discharge circuit inductance < 100 nH) and use the same disposable electrodes and focusing reflector dimensions. The first device, referred to as the experimental lithotripter, is described by Coleman et al. (1989). The second device is a commercial prototype based on the experimental lithotripter (manufactured by EEV Ltd., Lin-

coln) and is referred to here as the EEV lithotripter. Experiments on the acoustic and light emission were, for convenience, carried out independently on the experimental lithotripter at St. Thomas' Hospital, London, and the EEV lithotripter at the Cavendish Laboratory, Cambridge, respectively.

No significant difference is expected between the acoustic output of the two nominally identical sources. However, while it has been noted that the emission of multiple shocks by electrohydraulic sources is a reproducible feature, the delay between shocks is sensitive to the strength of the discharge, and slight differences in the delay between shocks are observed in successive discharges on the same source. Similar differences may be expected between delays from the two electrohydraulic sources used here.

The discharge strength is affected not only by the output setting but also by such factors as the size of the electrode gap and the water condition. At a constant output setting of 20 kV, the delay between primary and secondary shocks was found to increase from 3.1 ms to 4 ms in tap water as a new electrode ages (from 1 to 100 discharges). At the highest output setting using an old electrode, where the electrode gap has widened considerably, delays of 6 ms can be achieved. The standard deviation (SD) (expressed as a percentage of the mean of consecutive readings) for the delay between the primary and secondary shocks from discharges of the same source is 4% and corresponds to a variability in delay of about ± 150 μs for a typical 20 kV output setting using a new electrode. In addition to this random variation in primary to secondary shock delay, there is a systematic increase in the delay of about 900 μs as a new electrode ages over 100 discharges. Where nominally identical sources are operated at the same setting and with new electrodes, as here, the differences in the delay between primary and secondary shocks could reasonably be expected to be less than 900 μs although not better than the random variability of ± 150 μs.

Measurement of sound emission

Evidence in the literature (reviewed by Young 1989a) suggests that, for high drive levels, the acoustic emission from cavitation may be expected in the form of white noise generated at an intensity which dominates any detectable acoustic emission at harmonics of the driving frequency. This white noise generation is attributed to the emission of steep-fronted shocks by transient cavitation (Neppiras 1968).

A hydrophone having a wide bandwidth would be considered ideal for detecting white noise emission; however, in practice, focused hydrophones of sufficient sensitivity having a wide bandwidth are not readily available and for this study a commercially produced 1 MHz piezoceramic crystal of the desired type and shape was obtained.

The 1.65 mm thick (1 MHz thickness resonance) focal disc of lead zirconate titanate piezoceramic (PZT-PC4), manufactured by Morgan Matroc Ltd., Wrexham, with a 100 mm diameter and 120 mm focal length was mounted with electrical connections to both silvered surfaces for use as an air-backed hydrophone. The bowl has a focusing gain of the order of 1000, and the -6 dB focal region of the reception zone is about 5 mm long (in the axial direction) and 3 mm wide (in the focal plane).

This hydrophone was immersed in tap water and the beam focus was aligned with the focus of the experimental electrohydraulic shock wave generator operated at stated voltages with a new electrode (less than 100 shots) of the Dornier type. It was positioned with its axis of symmetry perpendicular to that of the shock wave source (Fig. 4a). The tank containing the source and hydrophone was lined with an anechoic matting, and the source was mounted on sound absorbent material.

The hydrophone cable was connected via a high pass filter with a 100 kHz lower band cut-off into the 1 Mohm (23 pF) impedance of a LeCroy 9450 digital oscilloscope with a $400 \cdot 10^6$ sample/s and Fast-Fourier Transform (FFT) capability. The high pass filter was employed to remove signals which appeared at the radial resonance of the hydrophone (18 kHz). Without the filter, the amplitude of the signal at the radial resonance (1 V) overwhelms that at the thickness resonance (1 mV) when the shock wave source is discharged. With the filter in place, the radial mode resonance is not observed.

Signals at 1 MHz were attributed to acoustic emissions from within the hydrophone reception zone, and it was assumed that there was no contribution to the 1 MHz signal direct from the shock wave source. This assumption is supported by the need for reasonable alignment of the hydrophone with the beam focus to obtain a detectable signal at 1 MHz. The signal at 18 kHz, on the other hand, is attributed to the direct effect of the generated shock wave field on the hydrophone. The oblique incidence of any pulse originating from the source is assumed to enhance the observed excitation of the hydrophone radial resonance.

An additional property of the acoustic field of an electrohydraulic source was noted, using a broadband hydrophone, as a signal in the frequency range 5 to 10 kHz of similar amplitude at all positions within the tank. This was identified as the "ringing" of the ellipsoidal reflector following a discharge. This, being at a similar frequency, is also expected to enhance the sig-

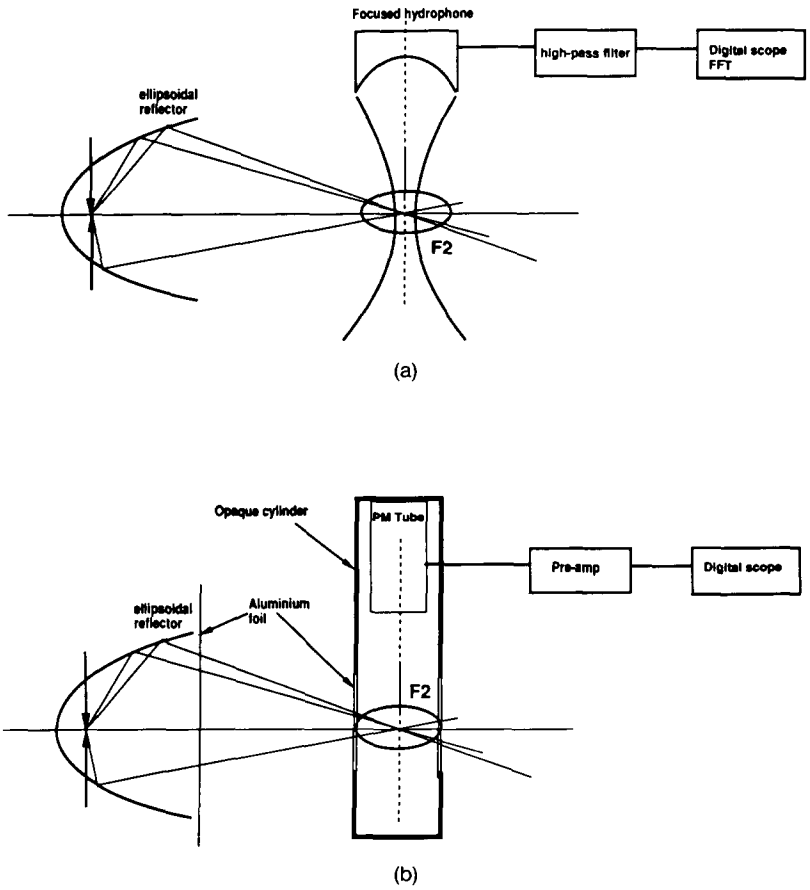

Fig. 4. The experimental set-up for (a) acoustic emission and (b) sonoluminescence measurements showing relative positions of the shock wave source and the hydrophone or PM tube, respectively, in an anechoic tank. The focus of the hydrophone is chosen to coincide with that of the shock wave source (F2). A high pass filter eliminates a relatively large amplitude signal at the radial resonance of the hydrophone (18 kHz). The PM tube is positioned within an opaque cylindrical container with acoustical windows made of aluminium foil. The ellipsoidal reflector is also shielded with aluminum foil to omit light produced by the electrical discharge.

nal picked up by the ceramic hydrophone at its radial resonance.

The open circuit, end-of-cable sensitivity of the hydrophone and filter system at 1 MHz was estimated from tabulated data to be 10 μV/Pa for a spherical wave emitted at the beam focus. The noise amplitude was less than 0.2 mV so that pressures above about 20 Pa could be expected to be detectable.

A relatively crude control experiment was carried out following all measurements with the hydrophone in which a 14-mm thick sheet of expanded polystyrene was placed in front of the aperture of the shock wave source. This thickness is able to attenuate the shock wave by more than −50 dB so that any signal still registered by the hydrophone could be identified as being unrelated to cavitation at the beam focus. In all cases, the observed signal at 1 MHz was suppressed, and only an electrical spike associated with the discharge was recorded.

Measurement of light emission

Light emission in the water around the beam focus of the shock wave source was examined using a fast PM tube (EMI 9789B) which has a 50-mm physical diameter and a 10-mm effective cathode diameter. The arrangement of the PM tube in the shock wave field is shown in Fig. 4b. The EEV lithotripter was used for this experiment and was operated at a setting of 20 kV. The PM tube output was connected to the LeCroy oscilloscope via a preamplifier. The special precautions necessary to shield the PM tube from the light flash which occurs at the moment of the electrical discharge made it difficult to obtain simultaneous measurements of light and sound emission as would have been ideal.

The reflector aperture of the shock wave source was covered by a plane sheet of 50-μm aluminium foil which transmits the shock wave with negligible attenuation but is opaque to the light of the discharge. The

PM tube was positioned out of the water with its front face 60 mm directly above the beam focus (F2) pointing into the water in a direction perpendicular to the acoustic beam axis (Fig. 4b). As additional protection from extraneous light, a thin cardboard cylinder (170-mm diameter) closed at both ends was placed in the water containing the beam focus. This cylinder was modified by cutting an aperture of 80 mm at one end to allow the PM tube a clear view of the focus and a 140-mm aperture covered with a double layer of aluminium foil in the side as a light opaque window for the acoustic beam. The PM tube, thus, viewed a volume of water surrounding the beam focus contained within a light opaque cylinder with an acoustic window. Care was taken to ensure that the aluminium foil remained opaque since it was found to become dented and eventually ruptured by the cavitation.

To identify any part of the detected signal which had an electrical origin, the 14-mm thick sheet of expanded polystyrene was inserted in front of the aperture of the shock wave source. A single electrical spike was observed to be associated with the electrical discharge of the source, but all signals following this were completely suppressed. As an additional control, water was drained from the tank at the end of the experiment so that the shock wave source fired in air. Again, no signal other than the initial electrical spike was obtained. This was interpreted as excluding the possibility that the PM tube was detecting light from the electrical discharge.

These experiments on the EEV lithotripter were later repeated on the experimental lithotripter. In this case an RCA 4880C/V2 PM tube was positioned and shielded as before with the output going via a preamplifier to the LeCroy oscilloscope. The experimental arrangement was otherwise unaltered. The results were essentially identical to those obtained previously although the time constant for the pulse decay on the RCA tube was about three times that from the EMI tube and the resulting traces appeared smoothed. Although these traces were more reproducible, the relative timing of signals is better resolved without smoothing and only results from the EMI tube are presented.

Water condition

Tap water contains sufficient particulate impurities to act as nucleation sites for cavitation and may, therefore, be expected to support cavitation relatively well (Keller 1972). In an attempt to verify the association between the hydrophone signal at 1 MHz and the presence of cavitation, an experiment was carried out in which the condition of the water was altered in a way that was expected to reduce the acoustic emission from cavitation without affecting the shock wave amplitude.

To suppress cavitation it was considered impractical to reduce the number of nucleation sites by, for example, filtering the water and an alternative approach was used. This approach is based on evidence that saturation of water with carbon dioxide gas, while lowering the cavitation threshold, inhibits cavitational collapse and consequently reduces acoustic and optical emission from cavitation. This effect is attributed to the high solubility of carbon dioxide gas which allows it more easily to diffuse into expanded bubbles and cushion their subsequent collapse (Young 1989b). The theoretical model described above confirmed this assumption for the case of a typical lithotripter pulse. For water containing 33 moles/m^3 of dissolved carbon dioxide, the predicted bubble response leads to a similar duration "quiet" period, t_c, but the amplitude of the acoustic emission from the second bubble collapse is predicted to be reduced by a factor of about 10 for both primary and secondary shocks.

The experiment to suppress cavitational collapse was attempted initially by filling the entire tank with carbonated water. It was found, however, that in the carbonated water the secondary shock was completely inhibited, presumably as a result of the alteration of the behaviour of the plasma bubble at the electrode gap. To overcome this problem the experiment was repeated with a thin (20 μm) polythene bag suspended in the anechoic tank so that the beam focus was contained within the bag. The bag was filled with the same amount of either tap water or carbonated tap water while the shock wave source operated in tap water in both cases. The hydrophone was placed in the same position as in Fig. 4a and remained outside the bag.

RESULTS

Comparison of sound and light emission

Figure 5a shows the oscilloscope trace of the 1-MHz signal registered by the hydrophone using the experimental lithotripter and Fig. 5b shows the oscilloscope trace obtained from the EMI PM tube using the EEV lithotripter. Both traces were recorded with an oscilloscope time base of 1 ms per division with a shock wave generator setting of 20 kV using a new electrode (*i.e.*, between 1 and 100 shocks). The oscilloscope sensitivity was set at 20 mV per division and 0.5 V per division for acoustic and optical traces, respectively, with the bar shown in each figure representing one division on both horizontal and vertical axes. In both cases the scope is triggered by the electrical

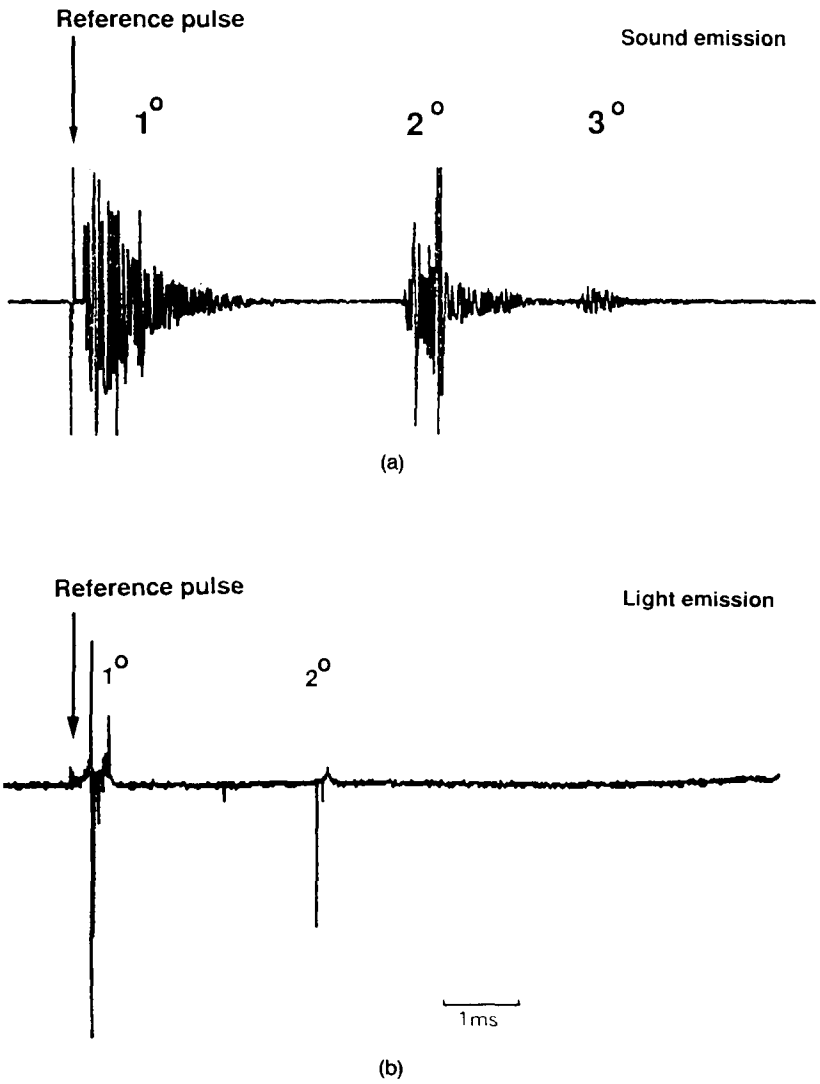

Fig. 5. Signal traces representing (a) 1-MHz sound and (b) light emission over a 10-ms period detected from a region around the beam focus of the two different (nominally identical) electrohydraulic shock wave sources following a single discharge of each source. The time delay between emission of primary (1°) and secondary (2°) shocks by each of the two sources is highly sensitive to the discharge strength, and the difference in the relative timing between the secondary shocks in (a) and (b) is within the variability expected (±900 μs).

spike which occurs at the moment of discharge and this acts as a reference pulse ($t = 0$) which is used to compare the timing of later signals.

The traces (Figs. 5a and b) show that there occur at least two distinct bursts of sound and light emission following the reference pulse which, from consideration of the relative timing of the pulses, can be associated with the arrival of the primary and secondary shock waves at the beam focus. The acoustic trace shows, in addition, a third burst associated with a third shock. The difference (of 400 μs) in the timing of the secondary acoustic and optical signal bursts (2° pulses in Figs. 5a and b) is within that expected from the random and systematic variations in delay between primary and secondary shock emission which is known to result from different discharge strengths generated by the two different shock wave sources.

In the acoustic trace (Fig. 5a) a signal burst (1°) occurs about 200 μs after the reference pulse. The maximum amplitude of this acoustic signal is about 0.005 MPa and falls roughly exponentially with a time constant of about 1 ms. There then follows a second signal burst (2°) of similar maximum amplitude associated with the arrival time of secondary shock at 3.9 ms after the primary shock. This second signal dies away, again roughly exponentially with a 1-ms time constant. Finally, there follows, 2 ms later, a signal burst of significantly smaller amplitude (3°) associated with the arrival at F2 of a third shock emitted by the source.

The optical trace (Fig. 5b) shares certain features with the acoustic trace (Fig. 5a). Following the reference pulse, the signal appears to build up slowly in amplitude over the 200 μs after which some large signal spikes appear. This signal burst (1°) is associated with the primary shock and lasts for less than 0.5 ms. A second signal burst significantly above the noise level (2°) occurs 3.5 ms after the onset of the first and is attributed, as in the case of the acoustical trace, to the arrival at F2 of the secondary shock. No third signal burst was observed.

Primary shock wave

Figures 6a and b show, respectively, details of the acoustic and optical traces associated with the primary shock wave. The time bases are both set to 200 μs per division so that, in both cases, the signal duration is 2 ms. This time scale allows better resolution of the delay between the reference pulse, on the left of each trace, and the onset of signal burst. Time differences can be resolved with an accuracy of about ±10 μs.

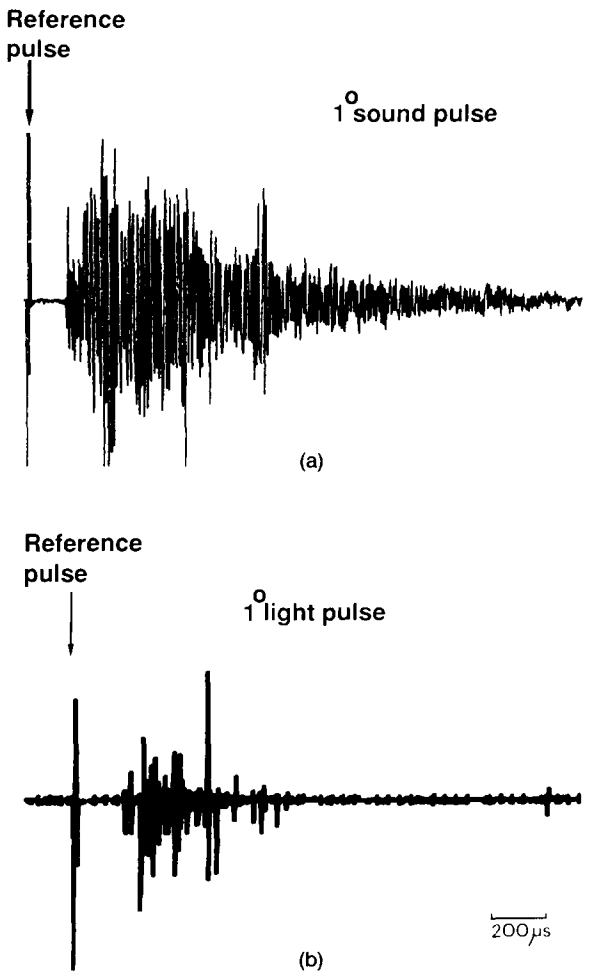

Fig. 6. Signal traces of (a) the 1-MHz sound and (b) the light emission over a 2-ms period due to the primary (1°) shock. These both show the expected delay between the reference (electrical) pulse and the commencement of sound and light emission during which the shock wave travels to F2. The time base is 200 μs/division.

The acoustic emission resulting from the primary shock, shown in Fig. 6a, has a complicated structure. The first signal above the noise level occurs 130 μs after the reference pulse. This time is too short to be attributed to a signal originating at the beam focus and is identified from its timing as the edge wave generated at the aperture of the reflector. Since the shock duration is 10 μs, no structure of the pulse itself can be resolved at this time base setting. At 260 μs after the reference pulse the acoustic signal peaks again. This delay corresponds with the time (180 μs) for the shock to travel from the source to the focus at F2 (Fig. 4a), a distance of 276 mm, plus the time for a signal to reach the hydrophone from F2 (80 μs), a distance of 120 mm and is, therefore, attributed to a source of sound originating at the beam focus. The signal then decays with a long (1 ms) time constant. Within this period there are various fluctuations in amplitude which do not appear to be particularly reproducible features.

The light emission due to the primary shock is shown in Fig. 6b. In this trace the reference pulse can be more clearly identified than in Fig. 5b. The first signal above the noise level occurs about 180 μs after the reference pulse and is attributed to light emission from the beam focus associated with the arrival of the shock wave at F2. As expected, therefore, the optical signal commences some 80 μs in advance of the sound signal, the difference representing the additional delay for the sound from F2 to reach the hydrophone. There is some indication of a decay in the underlying signal amplitude from a peak which occurs about 220 μs after the reference pulse. The time constant of this decay is about 100 μs.

Secondary shock wave

Figures 7a and b show details of the acoustic and optical signal bursts, respectively, both of which are associated with the secondary shock wave. The oscilloscope time base is set at 200 μs per division in both cases. These signals occur some 3 ms after the reference pulse which, obviously, does not appear on these traces.

The acoustic signal (Fig. 7a) shows a small initial spike which, as for the trace associated with the primary shock, is attributed to the arrival at the hydrophone of the edge wave. The main peak occurs 130 μs after the edge wave, the same delay as in the acoustic

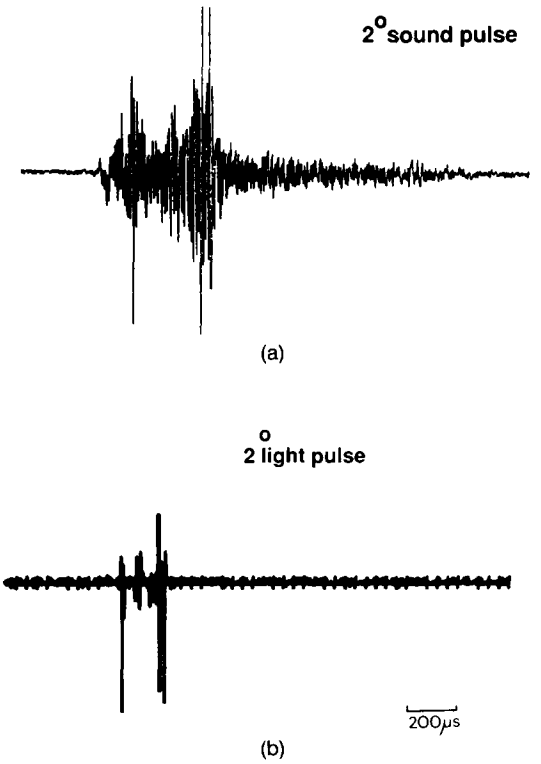

Fig. 7. Signal traces of (a) the 1-MHz sound and (b) the light emission over a 2-ms period due to the secondary (2°) shock. Both the sound and light emission have a similar structure showing two reproducible peaks separated by times of the order of 100 μs. The time base is 200 μs/division.

pulse from the primary shock and this peak is, therefore, attributed to an acoustic signal originating at F2. A small intermediate peak is followed by a large amplitude pulse which occurs 400 μs after the edge wave pulse. A long exponentially decaying signal with a 1-ms time constant then follows as in the acoustic signal from the primary shock.

The optical trace associated with the secondary shock (Fig. 7b) shows a similar structure to that of the acoustical trace with two main peaks with a small amplitude intermediate peak. The separation between the two main peaks in this case is 170 μs. There is no evidence, however, of the subsequent long decay period as seen in the acoustical trace. This signal is noticeably less reproducible than the acoustic signal and, in a series of 20 records, about one trace in three showed the three peak structure, the others showing only one or two of the peaks.

The durations of both acoustical and optical traces associated with the secondary shock (270 μs and 170 μs, respectively) are of the same order of magnitude as those predicted using the Gilmore model for the delay between the expected emissions from first and second bubble collapses, t_c, in response to a shock. The theoretical model also suggests that t_c increases with shock wave amplitude and it is, therefore, possible that the smaller (170 μs) delay measured for the light emission may result simply from the generation of a smaller amplitude shock by the particular source used in that experiment as indicated by the reduced separation between primary and secondary shocks (Fig. 5b).

A correlation between shock strength and the delay between the initial and second bubble collapses, t_c, is suggested by the theory and would, if verified experimentally, provide additional evidence that the separation of the peaks within a signal burst is associated with t_c. A further experiment was, therefore, carried out to examine this relation.

Signal variations with output setting

The time interval between the two main peaks within the acoustic trace associated with both primary and secondary shock waves was examined at different output settings of the shock wave generator in 1-kV steps over the range 15 to 25 kV using a new electrode. The time interval was more conveniently obtained from smoothed plots of the signal amplitude against time rather than from the signal itself. These plots were obtained relatively simply using the FFT facility of the LeCroy oscilloscope by obtaining the 1-MHz signal amplitude over a 100-μs record length and by stepping the 100-μs record at 10-μs intervals through the entire signal. At each interval the peak amplitude of the spread of amplitudes close to the resonant frequency was obtained. While a better signal-to-noise ratio could be obtained by integrating under the resonance curve either side of 1 MHz, this was not a convenient procedure and was unnecessary because the peak value of amplitude remained well above the noise level.

Plots of 1-MHz amplitude (in mV) against time for the acoustic signal associated with the primary shock are shown in Fig. 8 for 15-kV and 25-kV output settings of the Dornier HM3 type generator. The error bars indicate SD of a series of four repeated readings which, for the primary pulse, is found to be about 50% of the mean value.

Both graphs (in Fig. 8) show an initial increase in 1-MHz amplitude about 50–100 μs following the onset of the signal burst ($t = 0$). The initial peak in amplitude appears to be reproducible as does the final peak but in between these there are less reproducible peaks. The two plots in Fig. 8 illustrate that the separation of the first and final peaks increases with output setting of the generator. Repeated readings of separation at one output setting show a 25% variation. This corresponds closely to the expected pulse-to-pulse variation in shock wave amplitude, $p+$ (Coleman and

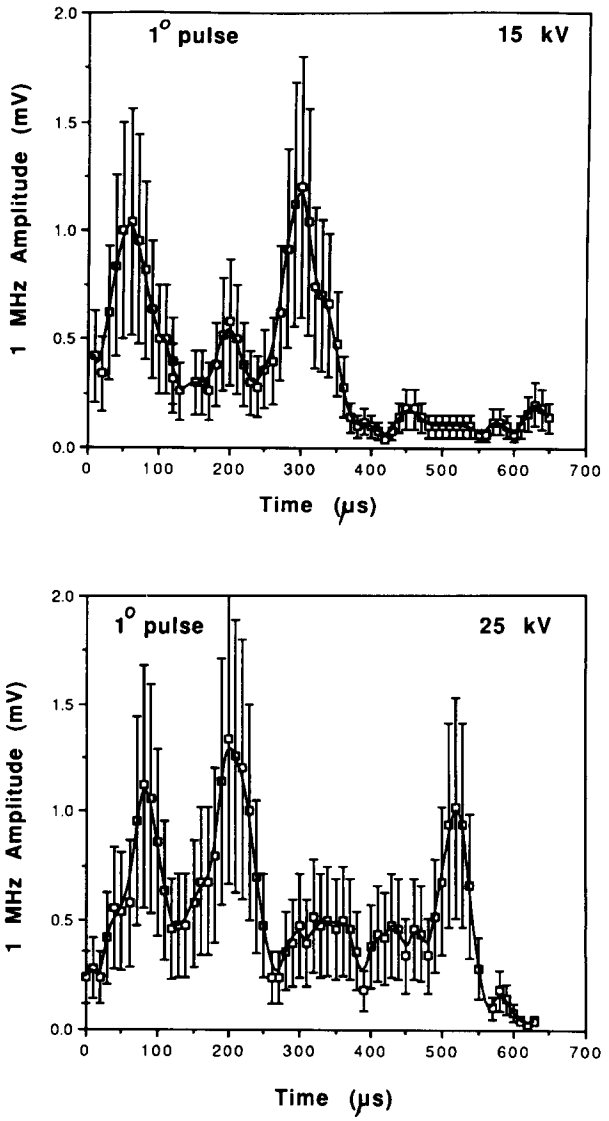

Fig. 8. Plots of the 1-MHz amplitude of the acoustic signal associated with the primary (1°) shock at source output setting 15 kV and 25 kV. These show an increase in signal duration with increased output setting. Error bars indicate the observed SD of 50% of the mean value.

Saunders 1989). At 15-kV separation of the peaks is 230 μs and increases to 430 μs at the 25-kV setting. Between 15 and 19 kV, there is little change in separation. Above 19 kV, the variation with voltage setting is approximately linear.

Plots of 1-MHz amplitude against time for the secondary shock are given in Fig. 9 for 15-kV and 25-kV settings. Error bars here represent the measured standard deviation of a series of four readings of about 40% of the mean value. The signal amplitude increases to a peak more than 50 μs after the first signal above the noise level. In this case, there are two clearly identifiable peaks which have a reproducible separation with little intermediate signal. The separation increases from 120 μs to 275 μs as the output increases from 15 kV to 25 kV.

The measured values of t_c obtained from plots of the signal burst following the secondary shock (as in Fig. 9) over the range 15–25 kV have been compared with theoretical predictions of t_c at different pressures ($p+$) made using the Gilmore model. Since the absolute value of $p+$ was not recorded in this experiment, it was necessary to convert the voltage setting to an estimated value for $p+$ due to the secondary shock in order to make the comparison. Using previous mea-

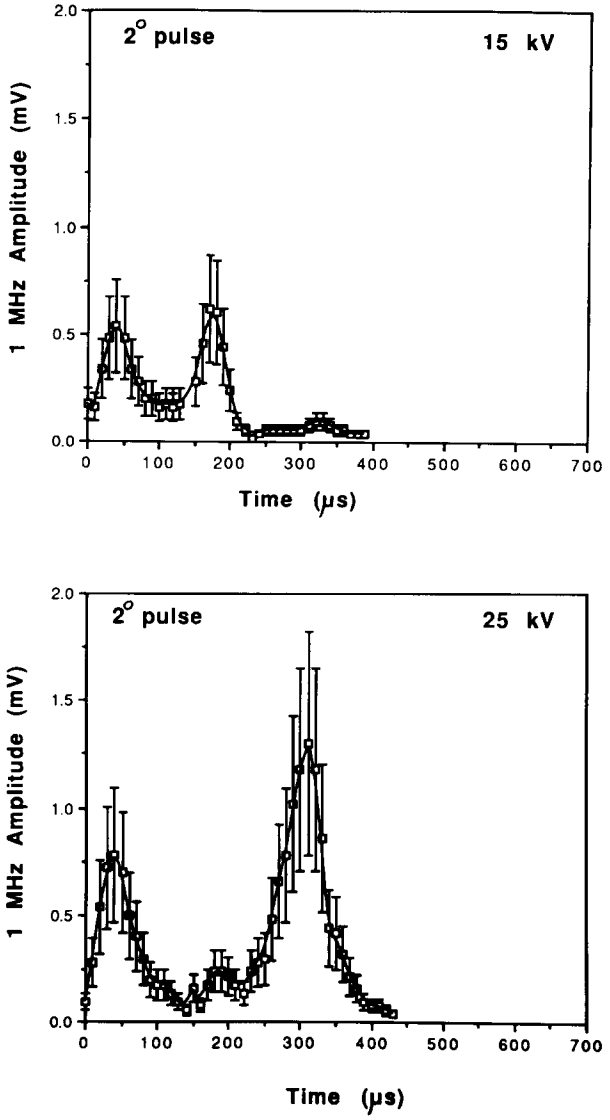

Fig. 9. Plots of the 1-MHz amplitude of the acoustical signal associated with the secondary (2°) shock at source output settings 15 kV and 25 kV. These show an increase in peak separation as well as an increase in amplitude at increased output setting. Error bars indicate the observed SD of 40% of the mean value.

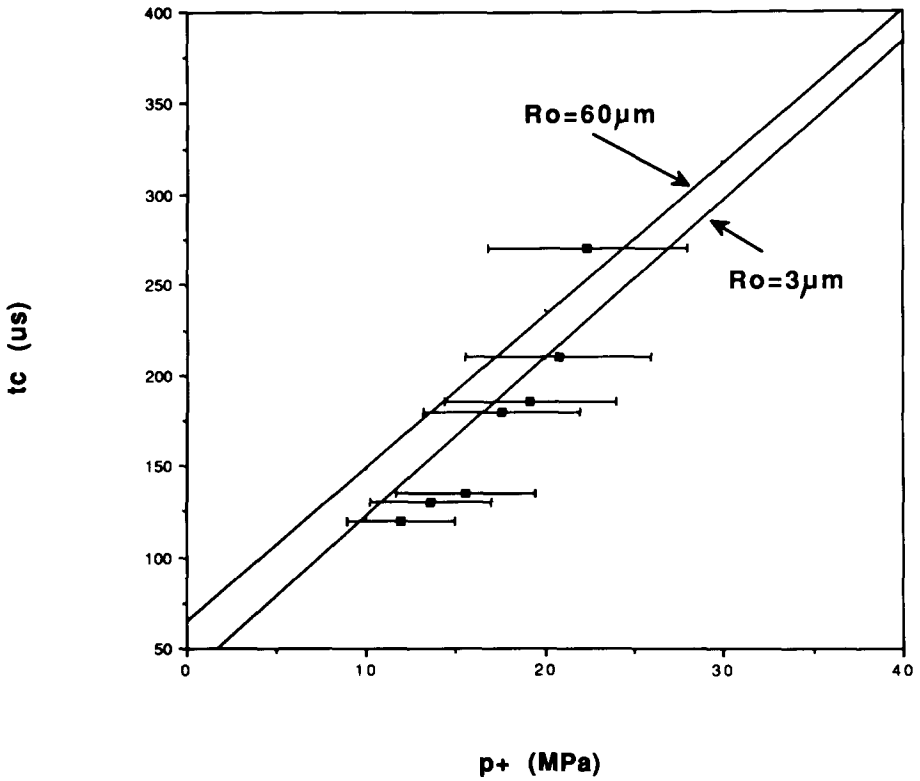

Fig. 10. A plot of the measured value of t_c (from the secondary shock) against shock amplitude estimated from the voltage setting. The error bars indicate the uncertainty in the estimated shock amplitude. The two solid lines indicate the theoretical variation of t_c with $p+$ for bubbles with initial radius (R_o) of 3 μm and 60 μm.

surements of the primary shock amplitude at the beam focus at different voltage setting (Coleman and Saunders 1989) the secondary shock amplitude, which is around 40% of that of the primary shock, can be estimated to be within about ±25%. The measured values of t_c at each voltage setting are plotted in Fig. 10 against the secondary shock amplitude estimated from the voltage setting with error bars indicating the estimated 25% uncertainty in $p+$. Measured values of t_c corresponding to voltages between 15 and 19 kV are all within ±20 μs of that for 15 kV and, for clarity, are represented by a single point in Fig. 10 at 120 μs. The solid lines indicate the theoretical predictions of t_c at a given shock amplitude using the Gilmore model for bubbles with initial radii 3 and 60 μm.

It is clear from Fig. 10 that, while the measurement of t_c can be made to within 5%, the large uncertainty in the estimation of $p+$ limits the use of t_c in obtaining reasonable estimates of bubble radius. This problem could be overcome by making simultaneous measurements of the secondary shock pressure waveform. While the absolute values of estimated $p+$ are subject to large errors since they were not directly measured, the graph in Fig. 10 does illustrate that the measured values of t_c increase in much the same way as predicted by the theory for any initial bubble radius.

Suppression of cavitation

The mean values of three consecutive readings of the 1-MHz amplitude obtained with the hydrophone directed at F2 in the bag containing tap water do not differ significantly from those shown in Figs. 8 and 9 for the primary and secondary shocks. In contrast, with carbonated water in the bag the mean values of three consecutive readings, 1-MHz amplitude at 10-μs intervals between 50 μs and 350 μs for the primary shock were less than 50% of those obtained in tap water. Similarly, for the secondary shock between 50 μs and 200 μs the mean 1-MHz amplitude was also more than 50% lower than was the case for tap water. In both cases the values outside this range did not differ significantly from those in tap water. At the relatively low signal-to-noise levels in the detected emission from carbonated water it was not possible to observe any structure in the signal such as the double peaks that are reproducibly noted in the emission from the secondary shock in tap water. The experiment is interpreted tentatively as indicating a reduced

acoustic emission from cavitation as a result of the enhanced diffusion of carbon dioxide into the bubble.

DISCUSSION

The sound and light emission from cavitation occurring near the beam focus of an electrohydraulic lithotripter have been examined using a hydrophone and a PM tube. It has been demonstrated that the hydrophone, which is placed outside the cavitation field, is capable of detecting acoustic emission from cavitation at the beam focus and that the timing and structure of the detected signal corresponds closely with the signal attributed to sonoluminescence obtained independently using a PM tube.

The correspondence between the time variation of the detected sound and light emission is taken as strong evidence that the focused hydrophone detects the acoustic emission from cavitation. Both sound and light emissions resulting from the primary shock indicate the generation of relatively incoherent signals of decaying amplitude as would be expected from the shock wave activation of a bubble population of widely varying initial radius. In contrast, the sound and light emission resulting from the secondary shock indicate the generation of coherent signals as might be expected from a population of similarly sized bubbles. The observation of differences in the coherence of the primary and secondary bubble response provides preliminary evidence supporting Church's (1989) prediction that diffusion tends to equalize the radii of bubbles exposed to lithotripsy shock waves of sufficient amplitude.

The reduced amplitude of the detected acoustic emission resulting from both the primary and secondary shocks in carbonated water provides additional evidence that the acoustic emission results from cavitation. This evidence is based on the model prediction that cavitational collapse will be cushioned as a result of increased gas diffusion into the bubble. The sonoluminescence generation, which was not examined in this case, would also be expected to be reduced.

On the assumption that the "quiet" period, t_c, is indeed measured by the separation of the peaks in the acoustic signal associated with the secondary shock it is possible, as suggested by Church (1989), that an estimate of bubble radius could be obtained provided a simultaneous measurement of $p+$ were made. The values of t_c measured here overlap with those predicted for bubble with radii within the range 3–60 μm. However, the large uncertainty in the estimation of the secondary shock amplitude and waveform, due to the lack of simultaneous measurements of pressure, makes it difficult to obtain more precise estimates of the bubble size. It should be noted that the model indicates that predicted values of t_c are more sensitive to negative peak pressure, $p-$, than to positive peak pressure, $p+$, and that, consequently, any simultaneous measurements of the secondary shock pressures should include the recording of $p-$ as well as $p+$.

CONCLUSIONS

This study demonstrates some qualitative aspects of cavitational activity occurring at the beam focus of an electrohydraulic shock wave lithotripter. The reasonable agreement between the experimental measurements of the time variation of the cavitation signals and those predicted using the Gilmore–Akulichev model of bubble dynamics provide encouragement that some useful quantitative information, such as the bubble radius, can be extracted.

Further studies of the detection of acoustic emission from cavitation might usefully examine the spectrum of the acoustic emission using a broadband hydrophone. This would allow some estimate of the likely attenuation of the signal by any intervening tissue if such a hydrophone were used to search for cavitation at depth in tissue. It might also allow identification of resonances such as that predicted following the main (second) bubble collapse at around 0.03 MHz which may allow some estimate of bubble size following the main bubble collapse.

The multiple shock output of an electrohydraulic lithotripter clearly influences the quality of the cavitational activity generated in these fields and may well influence the performance and safety of this type of lithotripter. With the increasing evidence that cavitation plays a role in stone fragmentation as well as in certain side effects of treatment, differences in the performance and safety of lithotripters, some of which generate single rather than multiple shocks, may well be more directly assessed by measurement of the quality of the cavitation fields which they generate than on the basis of the measurement of shock wave parameters alone.

Acknowledgements—The idea for this study arose from discussions with Dr. R. C. Preston and Dr. D. R. Bacon of the National Physical Laboratory to whom we are most grateful. We are also indebted to Professor C. R. Hill and Dr. G. R. ter Haar at the Institute of Cancer Research (Royal Marsden Hospital) for their advice and comments on the experimental work and to Professor R. L. Clarke for providing details of the piezoceramic crystal mounting. We are, similarly, indebted to Dr. J. E. Field of the Cavendish Laboratory, University of Cambridge, for his advice and comments on this study and Mr. R. Flaxman and Mr. D. Johnson, of the Cavendish, for their technical assistance with the light emission study. The computing work by Mr. Choi was supported on a Medical Research Council project grant and Dr. Leighton is supported by Magdelene College, Cambridge.

REFERENCES

Brummer, F.; Staudenraus, J.; Nesper, M.; Suhr, D.; Eisenmenger, W.; Hulser, D. F. Biological effects and physical characteriza-

tion of shock waves generated by an XL-1 experimental lithotripter. Ultrasound International 89 Conference Proceedings; 1989:1130–1135.

Church, C. C. A theoretical study of cavitation generated by an extracorporeal shock wave lithotripter. J. Acoust. Soc. Am. 86:215–227; 1989.

Coakley, W. T. Acoustic detection of single cavitation events in a focused field in water at 1 MHz. J. Acoust. Soc. Am. 49:792–801; 1971.

Coleman, A. J.; Saunders, J. E. A survey of the acoustic output of commercial extracorporeal shock wave lithotripters. Ultrasound Med. Biol. 15:213–227; 1989.

Coleman, A. J.; Saunders, J. E.; Choi. An experimental shock wave generator for lithotripsy studies. Phys. Med. Biol. 34:1733–1742; 1989.

Coleman, A. J.; Saunders, J. E.; Crum, L.; Dyson, M. Acoustic cavitation generated by an extracorporeal shockwave lithotripter. Ultrasound Med. Biol. 13:69–76; 1987.

Delius, M.; Denk, R.; Berding, C.; Liebich, H.; Jordan, M.; Brendel, W. Biological effects of shock waves: Cavitation by shock waves in piglet liver. Ultrasound Med. Biol. 16:467–472; 1990.

Flynn, H. G.; Church, C. C. A mechanism for the generation of cavitation maxima by pulsed ultrasound. J. Acoust. Soc. Am. 76:505–512; 1984.

Gambihler, S.; Delius, M.; Brendel, W. Biological effects of shock waves: Cell disruption, viability, and proliferation of L1210 cells exposed to shock waves *in vitro*. Ultrasound Med. Biol. 16:587–594; 1990.

Gavrilov, L. R.; Dmitriev, V. N.; Solontsova, L. V. Use of focused ultrasonic receivers for remote measurements in biological tissues. J. Acoust. Soc. Am. 83:1167–1179; 1988.

Hill, C. R.; Clarke, P. R.; Crowe, M. R.; Hammick, R. Ultrasonics for Industry Conference Papers. London: Iliffe Industrial Pub.; 1969:26–30.

Hunter, P. T.; Finlayson, B.; Hirko, R. J.; Voreck, W. C.; Walker, R.; Walck, S.; Nasr, M. Measurement of shock wave pressures used for lithotripsy. J. Urol. 136:733–738; 1986.

Keller, A. The influence of cavitation nucleus spectrum on cavitation inception, investigated with a scattered light counting method. Trans. ASME J. Basic Engng. 94:917–925; 1972.

Koch, H.; Grunewald, M. Disintegration mechanisms of weak acoustical shock waves. Ultrasound International 89 Conference Proceedings; 1989:1136–1141.

Miller, D. L. Ultrasonic detection of resonant bubbles in a flow tube by their second-harmonic emissions. Ultrasonics 19:217–224; 1981.

Neppiras, E. A. Subharmonic and other low-frequency emission from bubbles in sound-irradiated liquids. J. Acoust. Soc. Am. 46:587–601; 1968.

Nyborg, W. L.; Miller, D. L. Biophysical implications of bubble dynamics. Applied Scientific Research 38:17–24; 1982.

Riedlinger, R. Cavitation in the field of a focused pulsed high-power-sources: Photo documents and their relationship to biological effects. Proceedings of Workshop on biological effects and physical characterization of shock waves, Stuttgart. Unpublished; 1990.

Vaughan, P. W.; Leeman, S. Sonoluminescence: Violent light or gentle glow? IEEE Ultrasonics Symposium Proceedings, Williamsburg, VA, USA, 2:989–992; 1986.

Walton, A. J.; Reynolds, G. T. Sonoluminescence. Adv. Phys. 33:595; 1984.

Williams, A. R.; Delius, M.; Miller, D. L.; Schwarze, W. Investigation of cavitation in flowing media by lithotripter shock waves both *in vitro* and *in vivo*. Ultrasound Med. Biol. 15:53–60; 1989.

Young, F. R. Cavitation. Maidenhead: McGraw-Hill Book Company (UK) Ltd., 1989a:121–136.

Young, F. R. Cavitation. Maidenhead: McGraw-Hill Book Company (UK) Ltd., 1989b:359.